# EFFECT OF PRECURSORS AND WATER TO BINDER RATIOS ON THE WATER PERMEABILITY OF ALKALI-ACTIVATED MORTARS

**Thi Nhan Nguyen (1,2), Quoc Tri Phung (2), Lander Frederickx (2), Diederik Jacques (2), Alexandre Dauzeres (3), Jan Elsen (1), Yiannis Pontikes (1)**

(1) Department of Materials Engineering, KU Leuven, 3001 Leuven, Belgium

(2) Institute for Environment, Health, and Safety, Belgian Nuclear Research Centre (SCK CEN), Boeretang 200, 2400 Mol, Belgium

(3) IRSN, BP 17, 92262 Fontenay-aux-Roses, France

## Abstract

This work investigates the water permeability of alkali-activated materials (AAMs), which is one of the key transport properties beside the diffusivity to assess the material durability. The AAMs were produced from granulate blast furnaces slag (BFS) and metakaolin (MK) with various water/binder ratios of 0.35, 0.45, 0.55, and 0.75, 0.85, 0.95 for BFS and MK based AAMs, respectively. Herein, a direct method using a constant flow controlled by a syringe pump, which has been successfully applied on conventional concrete, was used to measure the permeability of the AAMs. Data was then compared with the OPC mortars with similar w/b ratios. The results reveal that the permeability of BFS activated mortars is comparable to the one of OPC mortars. Both BFS and MK based AMMs are highly sensible with the changes in w/b ratio. The higher the w/b ratio, the higher the permeability. The extent in changing permeability with w/b ratio is stronger for BFS compared to MK based AMMs. Furthermore, a correlation between water permeability and microstructure obtained by nitrogen adsorption of the investigated AAMs is highlighted, which indicates that the permeability of MK based mortars is mostly controlled by capillary pores, while gel pores significantly affect the permeability of BFS based mortars.

Keywords: Alkali-activated materials, granulated blast furnaces slag, metakaolin, water permeability, w/b ratio

## 1. INTRODUCTION

The performance of AAMs under several aggressive conditions has been intensively investigated such as acid attack, carbonation, chloride penetration, and efflorescence [1]. These degradation processes are caused by the mass transport of aggressive liquids, gases and ions from external environment through the material matrix [2, 3]. As a result, the degradation of materials is significantly affected by the transport properties, which define how fast the mass transport through the pore structure could be. Besides diffusivity, under an advective regime,

permeability is the key parameter to assess the durability of construction and building materials exposed to an aggressive environment [4, 5].

Unlike classical cementitious materials with a numerous studies on the permeability, the permeability data for AAMs is limited based on our knowledge [4, 6]. Furthermore, such reported permeability is also incomparable, stretching in a large range with water permeability coefficient $k$ (hereafter expressed as hydraulic conductivity) from $10^{-3}$ - $10^{-4}$ m/s in alkali-activated concretes (with coarse aggregate) to $10^{-9}$ - $10^{-13}$ m/s in alkali-activated mortars, due to the variety in examined precursors, activators, w/b ratio, and curing time [4, 7-10]. Probably the reported permeability for alkali-activated concretes is too high due to uncertainty in measurements (e.g. leaking) or the coarse aggregates are permeable. Specially, even with the similar material parameters, the permeability results are still different because of the difference in methods used to determine the permeability as illustrated by the permeability measurement on alkali-activated slag (AAS) using head constant pressure (direct method) reported by Shi compared to using beam-bending method in Blyth and Vichit's studies [4, 7, 11]. Therefore, there is a need to perform a comprehensive study on permeability of AAMs to provide additional data complimentary with the available data to build a permeability dataset for these newly developed materials. A short review of water permeability of AAMs is presented below in order to have an overview of the permeability of AAMs in comparison with OPC system.

### 1.1. Existing water permeability data of AAMs

Several studies have been conducted on the water permeability of AAMs as summarized in Table 1. The study of Shi et al. is considered as one of the first intensive research on permeability of AAMs in general and alkali-activated slag (AAS) in particular [7]. He measured the water permeability on OPC and AASs activated by sodium silicate/sodium carbonate using a head constant pressure. The results indicated that both AAS types had a lower water permeability than OPC. The permeability were $10^{-14}$ and $10^{-13}$ m/s for sodium silicate activated BFS, sodium carbonate activated BFS, respectively, compared to $5\times10^{-10}$ m/s for OPC sample. The lower permeability of AAS compared to OPC was also reported by Mithun [12]. However, few other studies showed a higher permeability in AAS than in OPC [13, 14]. It might be explained by the specific pore structure of examined materials, which directly controlled the permeable capacity. The pore structure of AAMs is not only affected by the water to binder ratio (w/b), but also by various factors including the precursor behaviours, activators, curing conditions. Therefore, it has been reported that the AAMs produced from low-calcium precursors such as fly ash and metakaolin (geopolymers) have elucidated a higher water permeability than OPC [8, 10], which is attributed to the more porous structure of these geopolymers compared to OPC matrix with the same w/b ratio.

Two main factors influencing the gel structure of materials and thereby the water permeability are the precursors used and the water to binder ratio. In terms of precursor, as shown in Table 1, N-A-S-H gel, which is formed by the activation of fly ash or metakaolin results in a higher water permeability due to its more porous structure compared to the one of C-A-S-H gel formed by the activation of slag. In the alkali-activated slag/fly ash blended materials, the increase of fly ash substitution leads to increase porosity and reduces tortuosity (because of more N-A-S-H is formed) as shown in the studies of Gao and Provis [15, 16]. Ismail also reported that fly ash content significantly affects the volume of permeable voids (VPV) of alkali-activated slag/fly ash blended mortars. The results showed that there is a limited change of VPV when fly ash content is lower than 50%, but VPV is significantly increased when the fly ash content exceeds 50% [17]. Besides, water permeability is remarkably influenced by w/b ratio. Higher w/b ratio leads to a larger permeability due to the larger pore volume and pore

size. The increase of w/b ratio in low-calcium fly ash based geopolymers results in a higher VPV and thereby a higher the water permeability. With low w/b ratios between 0.20 – 0.23, Olivia revealed that the permeability coefficient is in the range from $2.46 \times 10^{-11}$ to $4.67 \times 10^{-11}$ m/s corresponding to the VPV varying from 8.2% to 13% [18]. In case of geopolymer concrete produced from blends of rice husk-bark ash and fly ash, it exhibits a reasonably high water permeability of $6.79 \times 10^{-9}$ m/s for w/b ratio of 0.82 [8]. Besides, the water permeability is also affected by the interfacial transition zone (ITZ) between the matrix and aggregates. Ismail reported a higher VPV, thereby the permeability, of alkali-activated slag/fly ash blended concretes than mortars despite the fact that the paste volume fraction of mortars is higher than the one of concrete [17]. This implies that a coarser ITZ in concretes compared to mortars. Additionally, other factors such as curing time and temperature also may contribute to the permeability of AAMs like OPC because these factors affect the development of pore structure as well as the formation of cracks during polymerization, which significantly influence the water transport [19].

**Table 1: A summary of water permeability of AAMs reported in literatures**

| Precursors | Types of materials | w/b ratio | Curing time, days | Permeability (m/s) | Ref. |
|---|---|---|---|---|---|
| Rice husk-bark ash + fly ash | Concrete, (Fine aggregate) | 0.6-0.8 | 28, 90 | $10^{-10} \div 6\times10^{-9}$ | [8] |
| BFS | mortar | 0.485 | 7, 28 | $\sim10^{-13}$ | [7] |
| Fly ash | mortar | 0.4 | 7, 28, 90, 180 | $10^{-13} \div 10^{-10}$ | [10] |
| Metakaolin (MK)<br>BFS<br>MK+BFS | concrete | 0.38<br>0.6<br>0.4 | 7 | BFS's:<br>$1.3 \times10^{-3} \div 3\times10^{-4}$<br>MK's:<br>$1.4 \times10^{-3} \div 3\times10^{-4}$<br>(MK+BFS)'s:<br>$1.6 \times10^{-3} \div 4\times10^{-4}$ | [13] |
| Fly ash | concrete | 0.35<br>0.40<br>0.45 | 7 | $2\div 6 \times10^{-3}$ | [9] |
| Fly ash | concrete | 0.3 | 7 | $0.6 \div 1.3 \times10^{-3}$ | [20] |
| Fly ash (high calcium) | concrete | 0.45 | 7 | $0.7 \div 1.2 \times10^{-3}$ | [21] |

## 1.2 The current state and perspectives

Despite the importance of water permeability to evaluate durability of AAMs, there is only a limited dataset on permeability available as discussed above. The existing data is also not consistent and does not allow to establish any correlation between water permeability and gel/micro structure (e.g. porosity, pore size, tortuosity) as the case of cementitious materials [22, 23]. Therefore, there is a need to perform comprehensive studies and provide additional datasets which allows to correlate the microstructure and permeability of AAMs.

Most of existing techniques to measure permeability of cementitious materials could be used for AAMs as their similar characteristics with respect to the transport of fluids. The direct method with a constant water head pressure commonly used for OPC systems could be a relevant method for geopolymers because of the consistently obtained permeability on both

OPC materials and AAMs [6-8, 10]. Recently, beam-bending technique has been used to study on AAS and showed the similar permeability to OPC and lower values compared to AAS measured by the direct method in other studies [4]. The difference in permeability due to using various techniques once again elucidates the necessity of building a dataset for AAMs' permeability, which can be used as an important input for the prediction of durability of AAMs.

Considering limited dataset of AAM permeability available in literature, the main objective of the present study is to improve the knowledge on the effects of w/b and precursors on the permeability of AAMs. A novel constant flow was used to determine the permeability of AAS and alkali-activated metakaolin with different w/b ratios (i.e. 0.35-0.55 for AAS and 0.75-0.95 for alkali-activated metakaolin). Furthermore, the pore structure accessed by nitrogen adsorption are highlighted and used to correlate with the water permeability AAMs.

## 2. MATERIALS AND TEST SETUP

### 2.1. Raw materials and mixtures

The chemical compositions of BFS and MK used in the study are shown in **Table 2**. Sodium hydroxide 10 N and sodium trisilicate solution with 64.25% water were used as an activating solution. The fine river sand ($d_{max}$ = 2 mm) was used as a small fraction of 20% by volume. Tap water was used for mixing in this study. Three w/b ratios of 0.35, 0.45, 0.55 and 0.75, 0.85, 0.95 were investigated of AAS and MK-based geopolymers, respectively. Note that such w/b ratios were chosen in the context of immobilisation of radioactive liquid wastes, which is not discussed in this study. The binders here are referred to the total amount of precursor, solid sodium trisilicate and sodium hydroxide. The mix designs are presented in **Table 3**.

AAS and MK-based geopolymers specimens were produced by mixing BFS/MK with the activating solution, additional water and sand in a mortar mixer within around 10 minutes. The fresh geopolymers were then cast in cylindrical PVC tubes with the inner diameter of 97.5 mm. Herein, BFS 0.35, BFS 0.45, and BFS 0.55 denote for alkali-activated slag with w/b of 0.35, 0.45, and 0.55; while MK 0.75, MK 0.85, and MK 0.95 denotes for MK-based geopolymers with w/b of 0.75, 0.85, and 0.95, respectively. After casting, the specimens were sealed and cured at temperature of 20°C and relative humidity of 95% in a curing bench for 28 days.

**Table 2: Chemical composition of BFS and MK (wt.%)**

| Oxides | $SiO_2$ | $Al_2O_3$ | $Fe_2O_3$ | CaO | MgO | $K_2O$ | $Na_2O$ | $TiO_2$ | $SO_3$ | LOI |
|---|---|---|---|---|---|---|---|---|---|---|
| BFS | 32.4 | 11.1 | 0.60 | 43.40 | 7.77 | 0.53 | 0.27 | 1.01 | 2.41 | 2.08 |
| MK | 52.08 | 44.27 | 0.45 | 0.03 | 0.08 | 0.17 | 0.26 | 1.68 | 0.03 | 0.83 |

**Table 3: Mix compositions of BFS and MK-based geopolymers**

| w/b | BFS | MK | Silicate solution | Sodium solution | Additional water | Sand |
|---|---|---|---|---|---|---|
| | $kg/m^3$ | $kg/m^3$ | $kg/m^3$ | $kg/m^3$ | $kg/m^3$ | $kg/m^3$ |
| 0.35 | 955.5 | | 63.3 | 249.4 | 109.0 | 519.4 |
| 0.45 | 863.6 | | 57.2 | 225.4 | 190.6 | 519.4 |
| 0.55 | 790.1 | | 52.3 | 206.2 | 258.7 | 519.4 |
| 0.75 | | 863.6 | 637.9 | 389.8 | 127.7 | 519.4 |
| 0.85 | | 790.1 | 583.6 | 356.7 | 222.0 | 519.4 |
| 0.95 | | 735.0 | 542.9 | 331.8 | 304.2 | 519.4 |

## 2.2. Water permeability measurements

After 28 day curing, the samples were cut into small disks with the thickness of 25 mm by a diamond saw. The specimen were then saturated under vacuum water within 24 hours before embedding into a permeability cell. The sample preparation for the testing is described in details in a previous study on cement-based materials [6]. A photo and a schematic view of the experimental setup are shown in **Figure 1**.

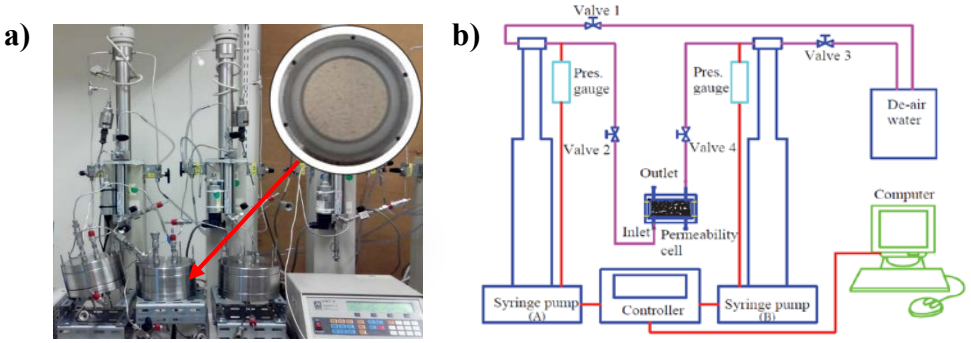


**Figure 1: A picture (a) and schematic view (b) of permeability setup adapted from [24]**

The testing procedure started from checking the leakage as well as removing entrapped air between lids and embedded samples by applying a water flow on each side of the permeability cell. Then, a pressure gradient was applied, which depends on each types of examined samples and their w/b ratios in order to ensure a high flow rate for high accuracy measurement but not create cracks in the samples due to high applied pressure. In all cases, the applied pressure was lower than 5 bar. Once a stable in-flow was achieved under a constant applied pressure, the testing system was switched to constant flow mode, and pressure was monitored until the difference in pressure between 2 measurements within 24 hours is smaller than 10%. The average pressure recorded within the last 24 hours was then used to calculate the water permeability coefficient using Darcy's law as follows [25].

$$K_w = \frac{Q \times H \times g \times \rho}{(A \times dP)}$$

where $K_w$= water permeability coefficient, m/s; $Q$ = rate of water flow, $m^3/s$; $H$ = thickness of the specimen, 0.025 m; $g$ = acceleration due to gravity, 9.81 $m^2/s$; $\rho$ = density of the water, 1000 $kg/m^3$; $A$ = the area exposed to water, 0.007462 $m^2$ (with diameter of 0.0975 m); $dP$ = average pressure gradient, Pa.

## 2.3. Characterization of microstructure

Nitrogen adsorption technique was used to define the specific surface area and quantify the pore sizes in the range from 3 to 70 nm. Samples after 28 days of curing were freeze-dried and then sieved at 500-800 µm before testing. The measurement was carried out with the TriStar 3020 device at temperature of 77K. The specific surface area was quantified by using BET method, which is applied to the adsorption isotherm, while the pore size distribution was

determined by the Barret-Joyner-Halenda (BJH) method for the desorption isotherm.

In addition, the water porosity was determined using a traditional saturation method.

## 3. RESULTS AND DISCUSSION

### 3.1. Water permeability results

The water permeability coefficients of examined AAMs are shown in **Figure 2**. As expected, the permeability decreases with the decrease of w/b ratios in both types of mortars activated from MK and BFS. Generally, higher w/b ratio results in a coarser pore structure of AAMs (i.e. higher porosity and larger pore size) [18, 26]. Especially, the capillary porosity, which controls the permeability of mortar due to composing of a plenty number of large and connected pores [10, 27], is also expected to be significantly increased with the increase of w/b ratio. Regarding to the influence of precursor, although the permeability of MK-based geopolymers is approximately 5 orders of magnitude higher than of AASs (i.e. $10^{-8}$ m/s compared to $10^{-13}$ m/s). The difference is attributed to not only the difference in precursor types but also the variation in w/b ratios. However, the latter is expected to largely contribute to permeability of the samples because much higher w/b ratios were used for activating MK than BFS.

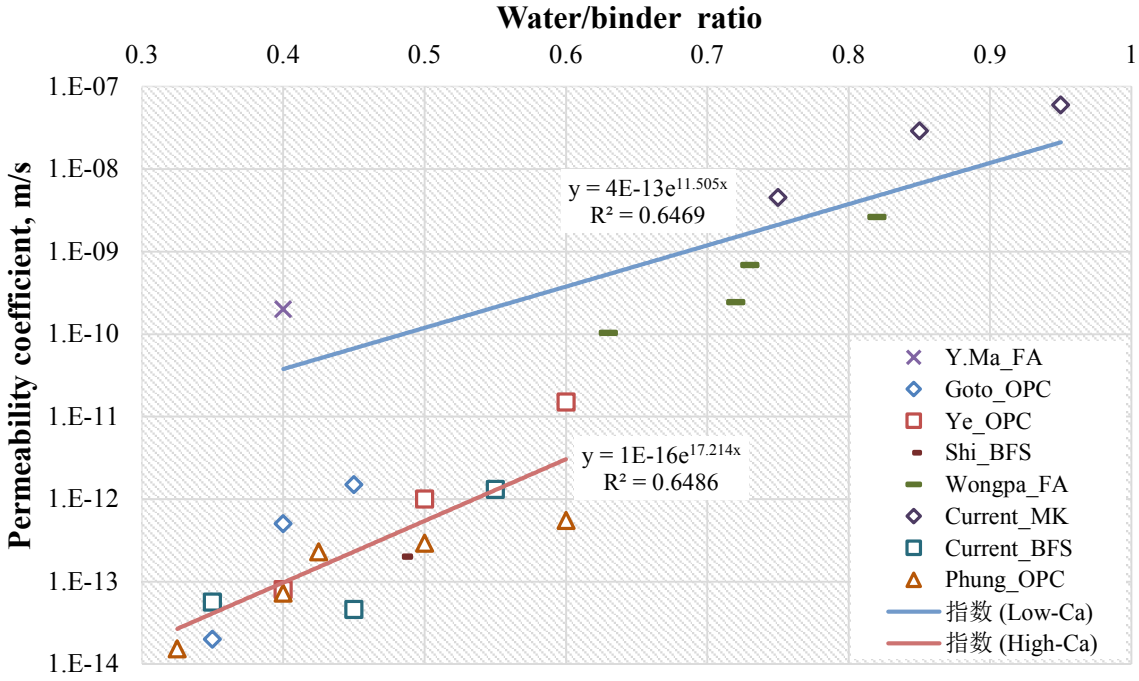


**Figure 2: Water permeability of current AAMs and from literature**

Figure 2 also shows the comparison of permeability measured in this study and data reported in the literature using direct methods [7, 8, 10, 27, 28]. In general, the current results are consistent with reported data, especially with AAS samples compared to results of Shi's study [7], which also examined with similar AASs and used a traditional testing method for permeability measurement. Besides, the permeability of AAS is very close to that of OPC materials, evidenced by a relatively high $R^2$ value of 0.65 for high calcium system including AAS and OPC (high-Ca). This indicates that the matrix of AAS can be as dense as that of OPC with the same w/b ratio. The results of obtained MK-based geoplymers are also in agreement with the data reported by Ma et al. and Wongpa et al. [8, 10], which examined with fly ash (FA) at a lower w/b range. There exhibits a slightly lower permeability of FA-based geopolymers

compared to MK-based geopolymers (this study), which can be attributed to the difference precursor behaviours such as its reactivity and pore size particles as well as the synthesis conditions leading to the difference in the extent of geopolymerization and thereby their pore structure. In addition, the higher Ca in FA than in MK may contribute to the denser structure of FA-based geopolymers compared to MK-based geopolymers [29]. Within a similar w/b ratio, it can be observed that the geopolymers produced from low-calcium precursors (e.g. MK and FA) exhibit a higher permeability than high-calcium ones (e.g. BFS). The difference can be up to 2-3 orders of magnitude depending on the w/b ratio. This can be explained by the more porous structure of N-A-S-H (from low-Ca precursors) compared to C-(A)-S-H structure produced from high-Ca precursors resulting in a higher porosity and lower tortuosity in N-A-S-H gel and higher VPV if BFS is substituted by FA in activated BFS/FA blend as reported in [15, 16].

### 3.2. Correlation between the water permeability and microstructure of AAMs

As mentioned above, the pore structure plays as a key role governing the water permeability of AAMs. Herein, the pore volume, pore size distribution, specific surface area (SSA), porosity obtained from $N_2$ adsorption tests are shown in Table 4. The pore volume, SSA and porosity as indicated here is mainly characterized for gel pores within the range of 3-70 nm. It is clearly shown in Figure 3 that the higher the w/b ratio of alkali-activated slag, the higher the pore volume. The water porosity, which is characterized for a wider pore size range, is also consistently increased with the increase of w/b ratio of AAS. The higher pore volume results in an increase in the water permeability which is consistent with the trend of permeability in all AASs discussed previously in section 1.1. Additionally, the pore size distribution of these samples slightly shifts to the larger pore size range with the increase of w/b ratio. The specific surface area obtained from BET method and porosity from BJH, presented in Table 4, also increase with the increase of w/b ratio.

**Table 4: Summary results from $N_2$ adsorption and water porosity test**

| Samples | BFS 0.35 | BFS 0.45 | BFS 0.55 | MK 0.75 | MK 0.85 | MK 0.95 |
|---|---|---|---|---|---|---|
| SSA (BET), $m^2/g$ | 5 | 15 | 21 | 11 | 7 | 3 |
| Porosity (BJH), % | 2.4 | 3.6 | 6.5 | 5.2 | 3.3 | 2.1 |
| Water porosity, % | 29.5 | 33.0 | 37.2 | 45.5 | 46.0 | 50.2 |

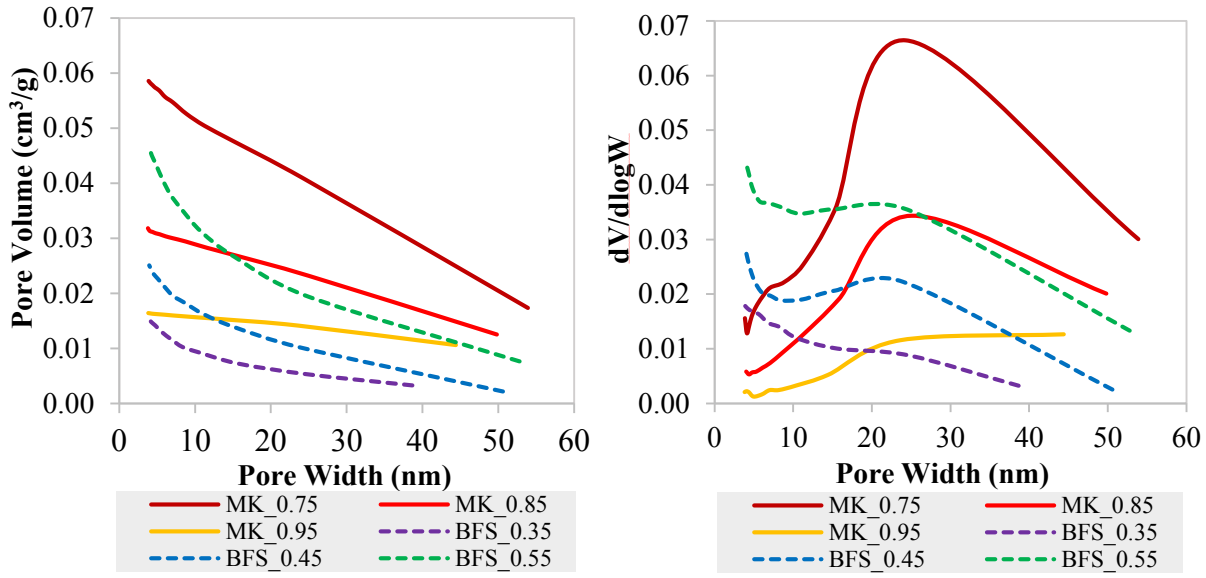


**Figure 3: Pore volume (a) and pore size distribution (b) of AAMs determined by $N_2$ adsorption**

In contrast to AAS, it is observed that the MK-based geopolymer with w/b ratio of 0.75 has the highest pore volume, SSA, and porosity (BJH), while showing the lowest water permeability. The permeability was $4.52 \times 10^{-9}$, $2.90 \times 10^{-8}$, $6.23 \times 10^{-8}$ m/s for samples with w/b ratio of 0.75, 0.85, 0.95, respectively. The effect of w/b ratio on the microstructure of low calcium geopolymers is not consistently reported in the literatures. Maricela et al. [30] showed an increase in water porosity with the increase in w/b ratio of MK-based geopolymers with a low water content, while Oliver et al. [31] reported a reduction in the gel pore volume (smaller than 30 nm) with the increase of w/b ratio for MK/FA-based geopolymers with a low water content. In addition, an increase in water porosity with the increase of w/b ratio was observed for MK-based geopolymers with high water content. In this study, we also observed a higher water porosity for higher w/b ratio geopolymers. However, the higher the w/b ratio, the lower the BJH porosity as shown in Table 4. Perhaps in a higher water content system as the case in this study, the dissolution of precursor and the mobility of alkali are increased with the increase of w/b ratio resulting in a higher N-A-S-H gel formation, which reduces the porosity at nano-scale. However, more water in the system would increase the capillary pore volume in hardened geopolymers. Furthermore, the gel porosity is significantly smaller compared to the water porosity. Therefore, the water permeability of MK-based geopolymers may be dominated by capillary pores rather than gel pores detected by $N_2$ adsorption [10].

## 4. CONCLUSIONS

In this study, the influence of precursors (i.e. metakaolin and BFS) and w/b ratios on the water permeability of alkali-activated mortars were elucidated. The results show that both factors have a significant effect on the water permeability of AAMs. AAS mortar exhibits a similar permeability compared to OPC system indicating a similar pore structure for both types of materials with the same w/b ratio. Higher w/b ratio results in a larger gel pore volume and total porosity determined by saturation method for BFS-based activated mortars. $N_2$ adsorption also indicates that the permeability of AAS is significantly controlled by gel pores. The higher the gel pore volume, the larger the water permeability. In contrast, MK-based mortars show an increase in the gel pore with the increase of w/b ratio, though the water porosity is still higher with the higher w/b ratio in MK-based mortars. The water permeability of MK-based mortars is also followed the same trend (i.e. higher w/b ratio results in higher permeability) as for AAS mortars, however, the extent in changing permeability with w/b ratio is stronger for BFS compared to MK-based AMMs. This implies that the permeability of MK-based mortars is mostly controlled by capillary pores. However, further analysis on pore structure (on-going work), which covers a wider pore size ranges (e.g. combined with mercury intrusion porosimetry and scanning electron microscopy) is needed to confirmed this hypothesis.

## ACKNOWLEDGEMENTS

This study has been funded by the Belgian Nuclear Centre (SCK CEN) and Institute for Radiological Protection and Nuclear Safety (IRSN).

## REFERENCES


1. Hu, X., et al., *Compressive strength, pore structure and chloride transport properties of alkali-activated slag/fly ash mortars.* Cement and Concrete Composites, 2019. **104**.
2. Albitar, M., et al., *Durability evaluation of geopolymer and conventional concretes.* Construction and Building Materials, 2017. **136**: p. 374-385.
3. Hossain, M.M., et al., *Durability of mortar and concrete containing alkali-activated binder with pozzolans: A review.* Construction and Building Materials, 2015. **93**: p. 95-109.
4. Blyth, A., et al., *Impact of activator chemistry on permeability of alkali-activated slags.* Journal of the American Ceramic Society, 2017. **100**(10): p. 4848-4859.
5. Guang, Y., *The microstructure and permeability of cementitious materials. PhD thesis*, in *Delft University of Technology, Delft*. 2003.
6. Phung, Q.T., et al., *Determination of water permeability of cementitious materials using a controlled constant flow method.* Construction and Building Materials, 2013. **47**: p. 1488-1496.
7. Shi, C., *Strength, pore structure and permeability of alkali-activated slag mortars.* Cement and Concrete Research, 1996. **26**(12): p. 1789-1799.
8. Wongpa, J., et al., *Compressive strength, modulus of elasticity, and water permeability of inorganic polymer concrete.* Materials & Design, 2010. **31**(10): p. 4748-4754.
9. Tho-in, T., et al., *Pervious high-calcium fly ash geopolymer concrete.* Construction and Building Materials, 2012. **30**: p. 366-371.
10. Ma, Y., J. Hu, and G. Ye, *The pore structure and permeability of alkali-activated fly ash.* Fuel, 2013. **104**: p. 771-780.
11. Vichit-Vadakan, W. and G.W. Scherer, *Measuring Permeability of Rigid Materials by a Beam-Bending Method: III, Cement Paste.* Journal of the American Ceramic Society, 2002. **85**(6): p. 1537-1544.
12. Mithun, B.M. and M.C. Narasimhan, *Performance of alkali-activated slag concrete mixes incorporating copper slag as fine aggregate.* Journal of Cleaner Production, 2016. **112**: p. 837-844.
13. Sun, Z., X. Lin, and A. Vollpracht, *Pervious concrete made of alkali-activated slag and geopolymers.* Construction and Building Materials, 2018. **189**: p. 797-803.
14. Bernal, S.A., et al., *Effect of binder content on the performance of alkali-activated slag concretes.* Cement and Concrete Research, 2011. **41**(1): p. 1-8.
15. Gao, X., Q.L. Yu, and H.J.H. Brouwers, *Assessing the porosity and shrinkage of alkali-activated slag-fly ash composites designed applying a packing model.* Construction and Building Materials, 2016. **119**: p. 175-184.
16. Provis, J.L., et al., *X-ray microtomography shows pore structure and tortuosity in alkali-activated binders.* Cement and Concrete Research, 2012. **42**(6): p. 855-864.
17. Ismail, I., et al., *Influence of fly ash on the water and chloride permeability of alkali-activated slag mortars and concretes.* Construction and Building Materials, 2013. **48**: p. 1187-1201.
18. Olivia, M. and H. Nikraz, *Strength and Water Penetrability of Fly Ash Geopolymer Conrete.* Journal of Engineering and Applied Sciences, 2011. **6**(7): p. 70-78.
19. Zhang, J., et al., *Durability of alkali-activated materials in aggressive environments: A review on recent studies.* Construction and Building Materials, 2017. **152**: p. 598-613.
20. Zaetang, Y., et al., *Use of coal ash as geopolymer binder and coarse aggregate in pervious concrete.* Construction and Building Materials, 2015. **96**: p. 289-295.
21. Sata, V., A. Wongsa, and P. Chindaprasirt, *Properties of pervious geopolymer concrete using recycled aggregates.* Construction and Building Materials, 2013. **42**: p. 33-39.
22. Phung, Q.T., et al., *Determination of water permeability of cementitious materials using a controlled constant flow method.* Construction and Building Materials, 2013. **47**(0): p. 1488-1496.
23. Phung, Q.T., et al., *Water permeability of cementitious materials: outstanding issues on measurement and modelling approaches*, in *2nd International RILEM/COST Conference on*

*Early Age Cracking and Serviceability in Cement-based Materials and Structures EAC-02*. 2017: Brussels, Belgium. p. 521-526.
24. Phung, Q.T., et al., *Effect of limestone fillers on microstructure and permeability due to carbonation of cement pastes under controlled CO2 pressure conditions.* Construction and Building Materials, 2015. **82**: p. 376-390.
25. Q.T. Phung, N.M., D. Jacques, G. De Schutter, G. Ye, *Effects of W/P ratio and limestone filler on permeability of cement pastes*, in *International RILEM Conference on Materials, Systems and Structures in Civil Engineering*. 2016.
26. Okada, K., et al., *Water retention properties of porous geopolymers for use in cooling applications.* Journal of the European Ceramic Society, 2009. **29**(10): p. 1917-1923.
27. Phung, Q.T., et al., *Investigation of the changes in microstructure and transport properties of leached cement pastes accounting for mix composition.* Cement and Concrete Research, 2016. **79**: p. 217-234.
28. Ye, G., P. Lura, and K. van Breugel, *Modelling of water permeability in cementitious materials.* Materials and Structures, 2006. **39**(9): p. 877-885.
29. Dombrowski, K., A. Buchwald, and M. Weil, *The influence of calcium content on the structure and thermal performance of fly ash -based geopolymers.* Journal of Materials Science, 2006. **42**(9): p. 3033-3043.
30. Lizcano, M., et al., *Effects of Water Content and Chemical Composition on Structural Properties of Alkaline Activated Metakaolin-based Geopolymers*. Journal of the American Ceramic Society, 2012. **95**(7): p. 2169-2177.
31. Vogt, O., et al., *Reactivity and Microstructure of Metakaolin -based Geopolymers: Effect of Fly Ash and Liquid/Solid Contents.* Materials (Basel), 2019. **12**(21).